JTEP Jurnal Keteknikan Pertanian,
Vol. 12 No. 3, p 362-375, 2024
P-ISSN 2407-0475 E-ISSN 2338-8439

Available online:
http://journal.ipb.ac.id/index.php/jtep
DOI: 10.19028/jtep.012.3.362-375

Box Design Selection for Portable Minapadi Based on Hydrostatic and Thermal Loading Simulation

Baskoro Tri Julianto[1*], Budi Indra Setiawan[1], Satyanto Krido Saptomo[1]

[1]Department of Civil and Environmental Engineering, Faculty of Agricultural Engineering and Technology, IPB University, Lingkar Akademik Street, IPB Dramaga Campus, Babakan, Bogor, West Java 16680, Indonesia
*Corresponding author, email: Baskoro.julianto46@gmail.com

Article Info

Submitted: 30 August 2024
Revised: 8 November 2024
Accepted: 25 November 2024
Available online: 26 November 2024
Published: Desember 2024

Keywords:
Box Simulation, Land Conversion, Portable Minapadi, Urban Farming, Young's modulus.

How to cite:
Julianto, B. T., Setiawan, B. I., Saptomo, S. K. (2024). Box Design Selection for Portable Minapadi Based on Hydrostatic and Thermal Loading Simulation. Jurnal Keteknikan Pertanian, 12(3): 362-375. https://doi.org/ 10.19028/jtep.012.3.362-375.

Abstract

Land conversions pose a threat to food security. Urban agriculture is considered to be a solution to this issue. Urban agricultural innovations are diverse, including vertiminaponics, cube-model microirrigation, and Nonpowered Automatic Fertigation systems. The development of a powerless automatic fertigation innovation involves creating a portable Minapadi concept by substituting some components, such as pots, with fiberglass boxes. This study aims to achieve a good box design to support the concept of urban agriculture. The study began by testing 10 fiberglass samples on a UTM machine to obtain the mechanical properties of the material, such as the modulus of elasticity, which were input into a computer simulator along with other physical and mechanical properties. The computer-aided simulator used was the ANSYS 2024 R2 Student software, simulating two potential box designs: the first box had a thickness of 4 mm with a lateral support in the middle of its vertical span, while the second box had a thickness of 6 mm without lateral support. Loading was applied hydrostatically with water level heights ranging from 50 to 400 mm and thermal loading simulating solar radiation. The results of this study show that solar radiation has a minimal impact on box deformation, whereas water-level height plays a significant role in box deformation. The first box design was considered the best based on deformation due to hydrostatic pressure, with a maximum deformation of 2.175 mm under hydrostatic loading with a water level height of 400 mm.

Doi: https://doi.org/10.19028/jtep.012.3.362-375

1. Introduction

Agricultural land conversion is a problem for agriculture and food security. For example, during the period 1994-2003 in Tangerang District, 5,407 hectares of agricultural land were converted from agricultural to non-agricultural use at a rate of 2.44 percent per year, which resulted in an average loss of rice production per hectare of converted land of 3,588.11 tons per year (Kadir, 2005).

Considering the example above, alternative agriculture is required to maintain food production. One such effort is urban farming, in which the concept of urban farming is to utilize narrow land in

JTEP Jurnal Keteknikan Pertanian,
Vol. 12 No. 3, p 362-375, 2024
P-ISSN 2407-0475 E-ISSN 2338-8439
Available online:
http://journal.ipb.ac.id/index.php/jtep
DOI: 10.19028/jtep.012.3.362-375

urban areas for agricultural purposes. One study stated that urban farming provides benefits to the community, both in the form of fulfilling nutritional needs, increasing family income, environmental aesthetics, and becoming a green open space in urban areas (Santoso et al., 2014).

Urban agriculture is a new field of study. As an example of its application, Rokhmah et al. (2014) created a Vertiminaponik model where the results showed that the developed Vertiminaponik model had a positive vegetable growth response and produced high yields. In addition, this study also showed the perception of cooperator farmers who stated that Vertiminaponik technology was considered more profitable than conventional cultivation. Imanudin et al. (2021) applied cube model micro-irrigation in yard land during the COVID 19 pandemic. The results of the application of this technology show that this cube model micro-irrigation system is highly efficient in water delivery, meets the criteria for water-saving irrigation, and utilizes durable local materials. In another concept, a subsurface irrigation system has been developed, in which water needs are adjusted to the evapotranspiration rate of plants. This system is referred to as an alternative irrigation system. The evapotranspirative irrigation system is called the Nirdaya Automatic Fertigator (FONi). Syafriyandi et al. (2023) tested the performance of Nonpowered automatic subsurface irrigation in the cultivation of three types of vegetable crops: kale, caisim, and spinach, where the plants were irrigated using a pipe connected to a cultivated plant pot. The results showed that this irrigation system model is highly effective, efficient, and easy to operate and maintain. Another development of this system was carried out by Muharomah et al. (2023), where the Nonpowered Automatic Fertigator (FONi) technology was applied in Tasikmalaya city, more precisely, at Madrasah Al-Manshur Tasikmalaya and the field laboratory of the UNSIL Tasikmalaya campus. Consequently, this technology can produce organic vegetables and meet consumer needs.

One of the developments in this technology is to make a portable Minapadi system, where the pots used will be substituted with fiberglass tubs. Problems arise when the quality and geometry of a tub are considered. The box was filled with water to a certain height to induce hydrostatic pressure, which caused deformation in the box. The hydrostatic pressure can be calculated by multiplying the fluid density function by the acceleration of gravity and the water level. Pratama et al. (2024) conducted a simple experiment on hydrostatic pressure where the experiment aims to find out the simple application of hydrostatic pressure with used bottle media by looking at the relationship between the number of water droplets and the depth of water with the duration of the experiment for one minute. This simple study proves that the height of the water affects the hydrostatic pressure, as evidenced by the number of water droplets. In addition to hydrostatic loads, thermal loads must be considered as an environmental effect in the form of exposure to sunlight. Usmani et al. (2001) describe that the total strain is the sum of the strain caused by thermal loads with mechanical strain where the thermal strain can be calculated by multiplying the coefficient of thermal expansion (α) with the

Available online:
http://journal.ipb.ac.id/index.php/jtep
DOI: 10.19028/jtep.012.3.362-375

change or increase in temperature (ΔT) described in a simple beam structure with roll-joint placement. Therefore, it is theoretically assumed that thermal loads affect the behavior of a structure when receiving physical loads. As a research example Panggabean et al. (2015) conducted research in the form of a comparison of the use of isotropic and orthotropic materials to analyze the strength of a ship's body made of fiberglass using the finite element method as a calculation and simulation method. The results of the study showed that the (orthotropic) method can provide quite detailed results, where the strength of each layer or laminate in the composite material can be described quite clearly and quite well. As an example of other research on the influence of thermal loads, Fauzi et al. (2019) analyzed the stability of slopes with woven geotextile reinforcement affected by thermal loads using the finite element method. Research has indicated that thermal parameters in the form of temperature and expansion are the most influential because they influence soil stability. In addition, a higher temperature affected the stability of the slope because the tensile strength of the geotextile decreased. Both studies proved that the strength of the material used for the construction of the equipment must be considered.

Based on the above explanation, it is necessary to review the structural strength of box-farming equipment. This study aimed to calculate and assess the influence of hydrostatic pressure and thermal loads on fiberglass agricultural boxes.

2. Research Methodology

The research began by testing the mechanical properties of fiberglass materials using a one-point loading bending test with a Universal Testing Machine (UTM). This single-point loading flexural test is based on the ASTM D790-17 standard test method for the flexural properties of unreinforced and reinforced plastics and electrical insulating materials. Research conducted by Utami et al. (2022). In this study, fiberglass samples were tested using as many as 10 homogeneous test samples with recapitulation of the test objects, as presented in Table 1 and sample photographs presented in Figure 1. The test object was placed on the UTM machine roll-joint inlet and loaded centrally at the middle of the span, as shown in Figure. 2.

JTEP Jurnal Keteknikan Pertanian,
Vol. 12 No. 3, p 362-375, 2024
P-ISSN 2407-0475 E-ISSN 2338-8439
Available online:
http://journal.ipb.ac.id/index.php/jtep
DOI: 10.19028/jtep.012.3.362-375

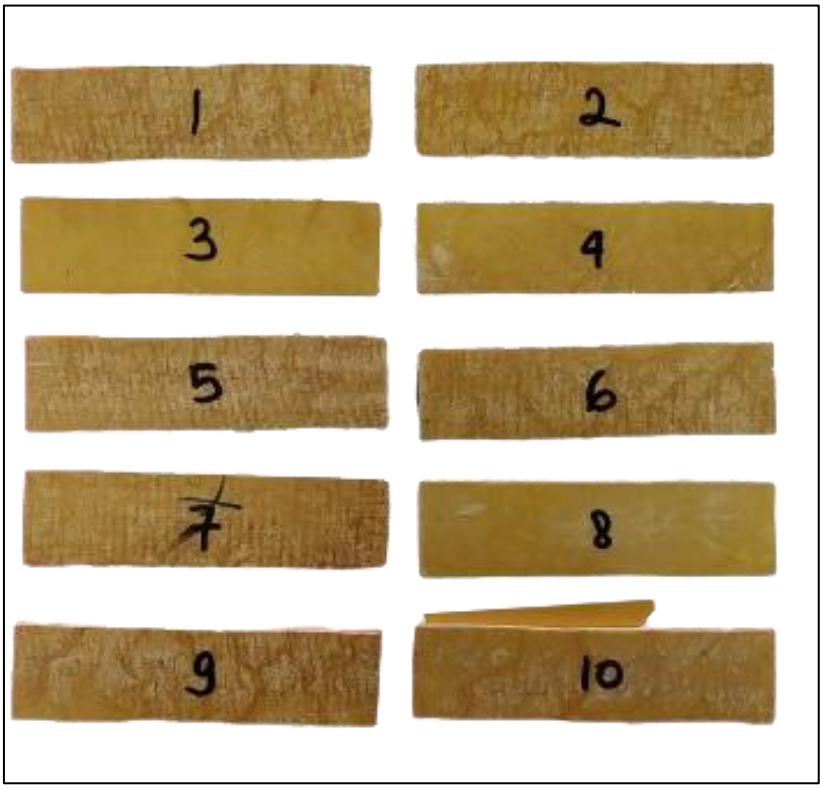

Figure 1. Example of Single Point Loading Flexure Test Piece

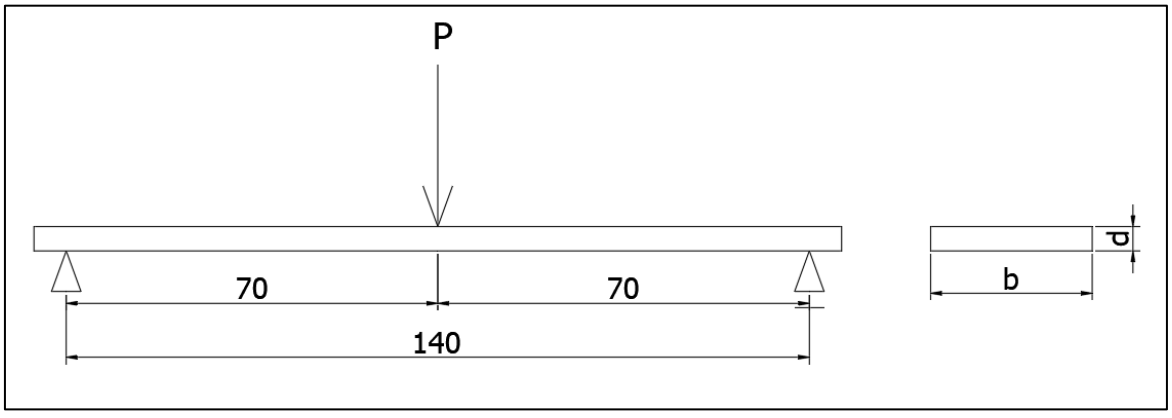

Figure 2. Schematic of Single Point Bending Test Loading

JTEP Jurnal Keteknikan Pertanian,
Vol. 12 No. 3, p 362-375, 2024
P-ISSN 2407-0475 E-ISSN 2338-8439
Available online:
http://journal.ipb.ac.id/index.php/jtep
DOI: 10.19028/jtep.012.3.362-375

Table 1. Single Point Loading Flexure Test Objects

Test Objects	Dimensions (mm)			Weight (gram)
	Width	Bold	Length	
1	39,90	4,90	151,30	62,21
2	40,10	4,70	152,00	62,18
3	40,70	4,70	150,50	63,85
4	39,60	4,90	151,10	61,84
5	39,00	4,60	151,20	61,74
6	39,10	4,70	150,90	61,36
7	39,70	4,50	152,20	60,43
8	40,90	5,00	151,30	65,18
9	39,60	4,70	151,50	60,46
10	39,00	4,80	151,20	60,30

The calculation of the mechanical properties consists of calculating the bending stress, bending strain, and modulus of elasticity as well as setting the loading muzzle motion speed, where the calculation successively follows Equations 1, 2, 3, and 4.

$$\sigma_L = \frac{3PL}{2bd^2} \quad (1)$$

Where σ_L is the bending stress (MPa), P is the load acting on the structure until the structure fails (N), L is the sample span length from support to support (mm), b is the sample width (mm), and d is the sample thickness (mm).

$$\varepsilon_L = \frac{6Dd}{L^2} \quad (2)$$

Where ε_L is the flexural strain ($mm.mm^{-1}$), D is the maximum deflection that occurs due to loading at the span center (mm), d is the sample thickness (mm) and L is the sample span length from support to support (mm).

$$E = \frac{L^3 m}{4bd^3} \quad (3)$$

Where E is the modulus of elasticity (MPa), L is the sample span length from support to support (mm), m is the gradient of the tangent to the initial straight line section of the load-deflection curve ($N.mm^{-1}$), b is the sample width (mm) and d is the sample thickness (mm).

JTEP Jurnal Keteknikan Pertanian,
Vol. 12 No. 3, p 362-375, 2024
P-ISSN 2407-0475 E-ISSN 2338-8439
Available online:
http://journal.ipb.ac.id/index.php/jtep
DOI: 10.19028/jtep.012.3.362-375

$$R = \frac{ZL^2}{6d} \quad (4)$$

Where R is the loading muzzle movement speed (mm/min), Z is the strain rate of the outermost fiber of the specimen (0.01 mm/mm/min), L is the span length from support to support (mm), and d is the thickness of the specimen (mm).

The next stage involves modeling the hydrostatic pressure and thermal loads with the help of ANSYS 2024 R2 Student software with an analysis system using a static structure, where Engineering Data uses data from one-point loading bending tests with the assumption that the material is an isotropic material with a Poisson value assumed to be 0.33, as recommended by Morgolis (2006). The thermal conductivity of the material (k) is assumed to be 0.035 W/mK, as described in SNI 6389:2020, and an anisotropic thermal expansion coefficient (α) of 6.3×10^{-6} 1/k in the x direction and 2×10^{-5} 1/k in the y and z directions, respectively, as described by Bayat (2023). The heat flow for the condition of irradiation to the inside of the box was approximately 854 Watts, while that for the condition of only the top of the box was 10,248 Watts. This value depends on the area exposed to radiation, where the condition of irradiation inside the box is assumed to have a larger heat-receiving area than the condition of only the top of the box. The heat transfer coefficient value for air (300 psig) was close to 60 Btu/h ºF ft² or 340.7 W/m² ºC, whereas for water (2.0 cP), it was 250 Btu/h ºF ft² or 1419.6 W/m² ºC, as explained by Steawart Jr. (2014). The hydrostatic loads were simulated at water levels of 50, 100, 150, 200, 250, 300, 350, and 400 mm. The structure was considered to be a monolith with two geometries. The first geometry had dimensions of 2000 mm × 1000 mm with a height of 400 mm, and there was lateral support at the mid-span height of the box geometry with lateral support dimensions of 40 mm × 40 mm. In addition to the midspan height, another lateral support with a thickness of 4 mm was installed at the mouth of the box. The second geometry was made without lateral support with a thickness of 6 mm, where the length, width, and height dimensions were identical to those of the first geometry model.

Simulations were carried out on two geometries, with each geometry applying two thermal load treatments, namely, the load given to the top of the ear and the inside of the box (thermal loading condition 1) and the load treatment only on the top of the ear of the box (thermal loading condition 2), as shown in Figure 5. The rice planting scheme was carried out in polybags, as shown in Figure 6.

JTEP Jurnal Keteknikan Pertanian,
Vol. 12 No. 3, p 362-375, 2024
P-ISSN 2407-0475 E-ISSN 2338-8439
Available online:
http://journal.ipb.ac.id/index.php/jtep
DOI: 10.19028/jtep.012.3.362-375

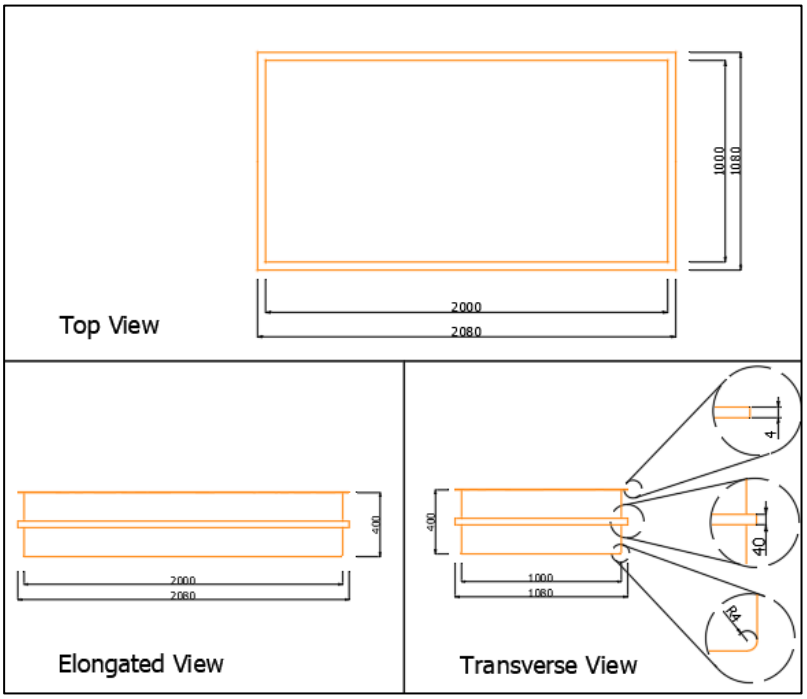

Figure 3. First Box Design (Dimensions in mm)

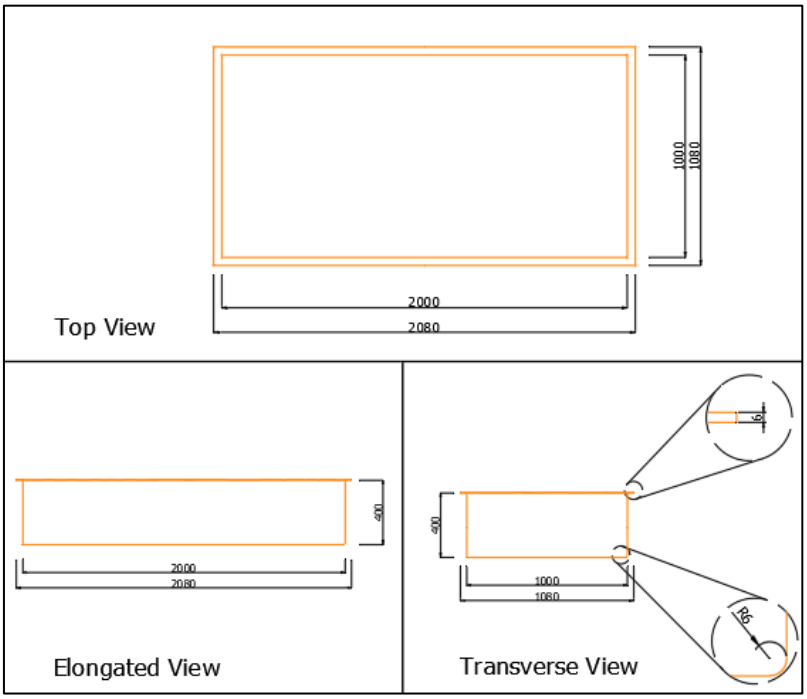

Figure 4. Second Box Design (Dimensions in mm)

JTEP Jurnal Keteknikan Pertanian,
Vol. 12 No. 3, p 362-375, 2024
P-ISSN 2407-0475 E-ISSN 2338-8439
Available online:
http://journal.ipb.ac.id/index.php/jtep
DOI: 10.19028/jtep.012.3.362-375

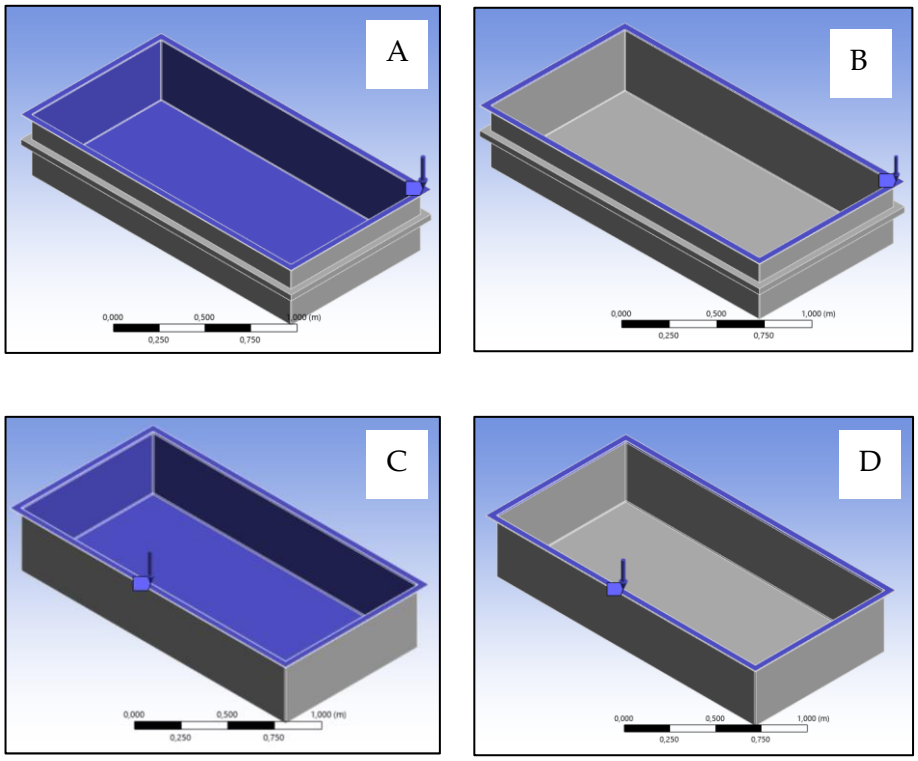

Figure 5. Thermal Loading Schemes Marked in Purple A) Design 1 with Thermal Loading Condition 1, B) Design 1 with Thermal Loading Condition 2, C) Design 2 with Thermal Loading Condition 1, D) Design 2 with Thermal Loading Condition 2

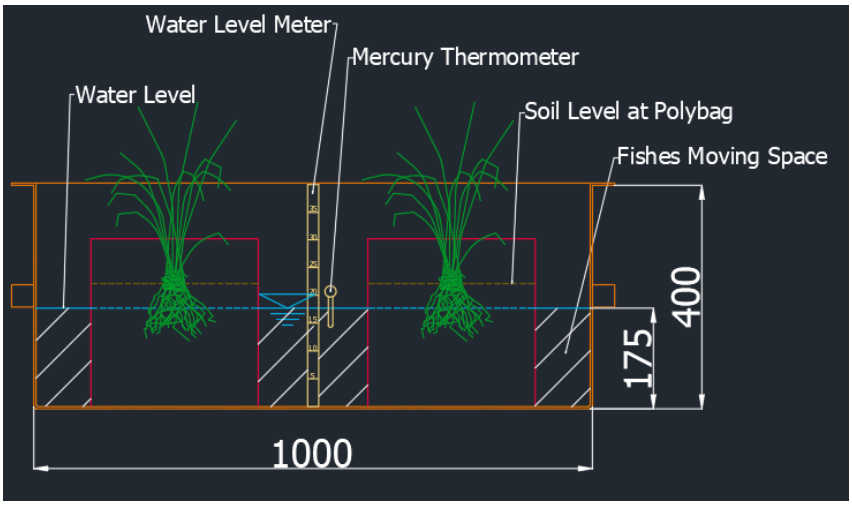

Figure 6. Schematic of Planting Location and Fish Movement Space in One Portable Minapadi System Box

JTEP Jurnal Keteknikan Pertanian,
Vol. 12 No. 3, p 362-375, 2024
P-ISSN 2407-0475 E-ISSN 2338-8439
Available online:
http://journal.ipb.ac.id/index.php/jtep
DOI: 10.19028/jtep.012.3.362-375

3 Results and Discussions

3.1 Mechanical Properties Testing og Fiberglass Samples

Testing using the UTM resulted in the load-deflection curve acting on the structure presented in Figure 7.

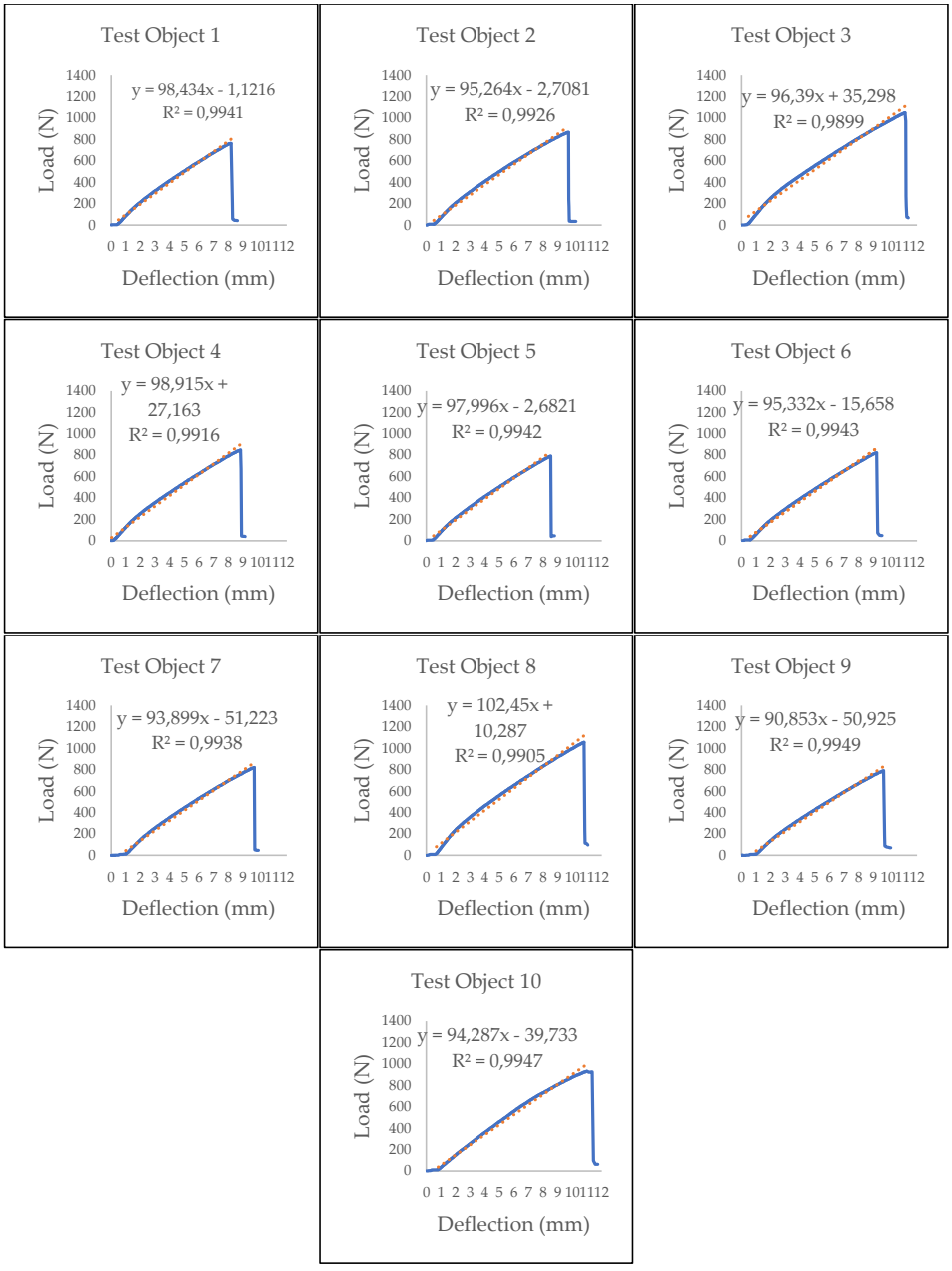

Figure 7. Load-Deflection Curve from UTM Readings

JTEP Jurnal Keteknikan Pertanian,
Vol. 12 No. 3, p 362-375, 2024
P-ISSN 2407-0475 E-ISSN 2338-8439
Available online:
http://journal.ipb.ac.id/index.php/jtep
DOI: 10.19028/jtep.012.3.362-375

In Figure 7, the blue line shows the data read by the UTM, and the orange dashed line is the linear regression of the gradient of the tangent line to the initial straight-line portion of the load-deflection curve. Based on the deflection and load relationship curves, it can be said that fiberglass is a brittle material characterized by the Ultimate Tensile Stress value at the same point as the Fracture Stress. The gradient of the tangent line to the initial straight-line part of the load-deflection curve was obtained by approaching the resulting linear equation shown by the gradient value of the equation. This value was calculated using the elastic modulus values listed in Table 2.

Table 2. Modulus of Elasticity of Fiberglass Test Samples

Test Objects	Dimensions (mm)			Density	R	m	E
	b	d	L_{Span}	(kg/m^3)	(mm/min)	(N/mm)	(MPa)
1	39,90	4,90	140,00	2103,03	6,67	98,43	14384,94
2	40,10	4,70	140,00	2170,42	6,95	95,26	15696,94
3	40,70	4,70	140,00	2217,85	6,95	96,39	15648,33
4	39,60	4,90	140,00	2109,01	6,67	98,92	14564,74
5	39,00	4,60	140,00	2276,11	7,10	98,00	17709,01
6	39,10	4,70	140,00	2212,51	6,95	95,33	16109,89
7	39,70	4,50	140,00	2222,32	7,26	93,90	17805,62
8	40,90	5,00	140,00	2106,60	6,53	102,45	13746,84
9	39,60	4,70	140,00	2144,12	6,95	90,85	15159,14
10	39,00	4,80	140,00	2130,43	6,81	94,29	14996,42
Avarage	39,76	4,75	140,00	2169,24	6,88	96,38	15582,19

In Table 2, it can be seen that the physical properties of the test samples are quite varied with an average width of 39.76 mm, an average thickness of 4.75 mm, and an average density of 2169.24 kg/m3. The average muzzle movement speed was 6.88 mm/min while the elastic modulus value obtained also varied significantly, with the largest elastic modulus value in sample No. 7 (17805.62 MPa and the smallest in sample No. 8 (13746.84 MPa and an average elastic modulus of 15582.19 MPa.

3.2 Hydrostatic Pressure Simulation

Simulations were carried out by defining the fiberglass material as an isotropic material with average density and elastic modulus values as presented in Table 2 which are 2169.24 kg/m3 and 15582.19 MPa, respectively. Based on the value of elastic modulus and Poisson's number of 0.33, the bulk modulus and shear modulus values can be calculated analytically following Equation 5 and Equation 6 (Hariandja, 1997) with bulk modulus and shear modulus values from analytical calculations being 15276.66 MPa and 5857.97 MPa, respectively.

Available online:
http://journal.ipb.ac.id/index.php/jtep
DOI: 10.19028/jtep.012.3.362-375

$$G = \frac{E}{2(1+\nu)} \quad (5)$$

$$K = \frac{E}{3(1-2\nu)} \quad (6)$$

Where G is the shear modulus (MPa), K is the bulk modulus (MPa), E is the elastic modulus (MPa), and ν is Poisson's number.

Both designs were checked for weight and volume using the ANSYS 2024 R2 Student software. The weight was obtained from the average material specific gravity in Table 2 multiplied by the calculation of the volume of the box, where the volume is the estimated cubication of the material used when the box is made. The weight of the first and second design boxes are 78.96 kg and 86.12 kg respectively while the volume of the box material is 0.0364 m3 and 0.0397 m3 respectively. It can be observed that the first design has a smaller weight than the second design, and the use of materials in the first design is less than that in the second design. Both designs were divided into strains, where the first design was divided into 112,665 strains and the second design was divided into 105,134 strains.

A hydrostatic pressure load was applied and the resultant force was calculated. The force was considered a triangular uniform load acting at 1/3 of the water level measured from the bottom of the box. The hydrostatic pressure and the force resulting from the hydrostatic pressure were calculated using Equations 7 and 8, respectively.

$$P = \rho g H \quad (7)$$

$$F = \frac{1}{2} PBH \quad (8)$$

Where P is the hydrostatic pressure (MPa), ϱ is the weight of the fluid content (kg/mm3), g is the acceleration of gravity (≈ 9810 mm/s2), F is the resultant force due to hydrostatic pressure (kgf.mm.s-2), B is the width of the container (mm) and H is the height of the water level measured from the bottom of the box (mm). The resultant hydrostatic force is calculated based on two directions, namely the x- and z-directions, where the container widths in the x- and z-direction orientations are 1000 mm and 2000 mm, respectively. The magnitude of the force caused by the hydrostatic pressure is shown in Figure 8.

JTEP Jurnal Keteknikan Pertanian,
Vol. 12 No. 3, p 362-375, 2024
P-ISSN 2407-0475 E-ISSN 2338-8439
Available online:
http://journal.ipb.ac.id/index.php/jtep
DOI: 10.19028/jtep.012.3.362-375

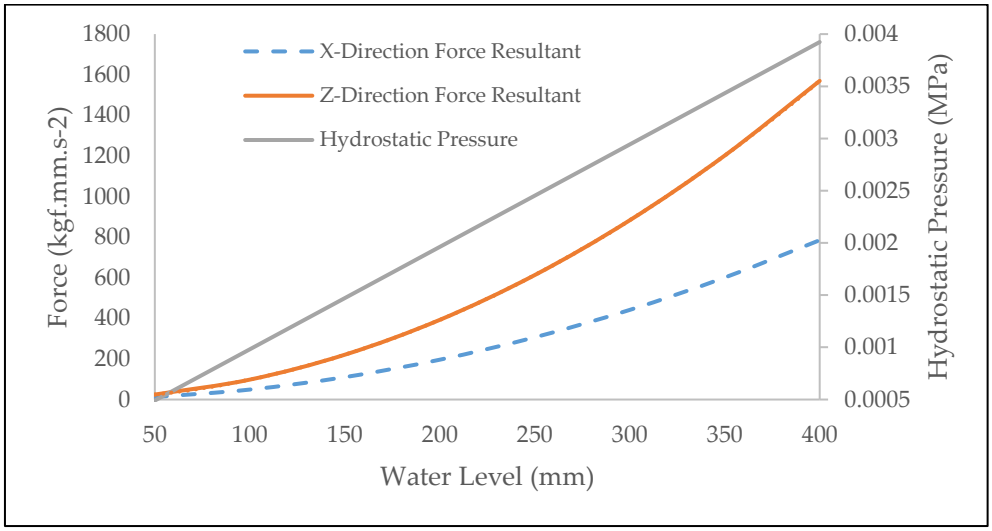

Figure 8. Resultant Force Magnitude Due to Hydrostatic Pressure

In the graph presented in Figure 8, the resultant force in both the x- and z-directions forms a quadratic equation, whereas the hydrostatic pressure forms a linear equation, both of which have an abscissa in the form of the water level. The largest force resultant is the force resultant at the maximum water level of 400 mm where the values for the x-axis and z-axis are 784.80 kgf.mm.s-2 and 1569.60 kgf.mm.s-2, respectively, both of which are generated from a hydrostatic pressure of 0.00392 MPa. The simulation results of the deflection due to hydrostatic pressure represented by the water level, which is also affected by the thermal load, are presented in Figure 9 and Table 3.

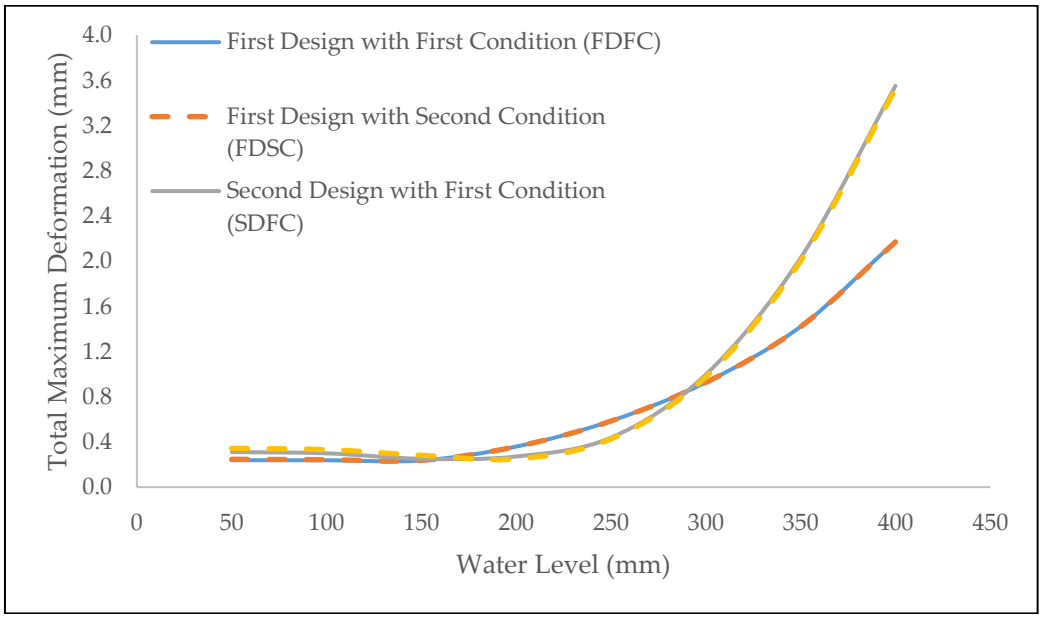

Figure 9. Total Deformation Magnitude due to Water Level Rise

Available online:
http://journal.ipb.ac.id/index.php/jtep
DOI: 10.19028/jtep.012.3.362-375

Table 3. Maximum Total Deformation Value due to Water Level Height

Water Level (mm)	Total Maximum Deformation (mm)			
	FDFC	FDSC	SDFC	SDSC
50	0,239	0,247	0,311	0,343
100	0,238	0,244	0,300	0,332
150	0,236	0,237	0,252	0,283
200	0,359	0,358	0,272	0,250
250	0,586	0,585	0,438	0,427
300	0,927	0,926	0,996	0,975
350	1,421	1,420	2,029	2,003
400	2,175	2,170	3,552	3,525

Figure 9 and Table 3 show the total deformation owing to hydrostatic pressure, represented by the water level of the two designs. The first box design exhibited a smaller total deformation than the second box design at a maximum height of 400 mm. However, at a certain water level, the deformation of the first box design was greater than that of the second. The two thermal loading conditions did not have a significant influence on the thermal load conditions in either the first or second box designs, which were not significantly different. It can be said that thermal loading does not affect the total deformation arising from the hydrostatic pressure. This indicates that the fiberglass box can be said to be quite resistant, especially to deformation caused by environmental loads in the form of thermal loads.

4. Conclusion

Based on the results of research conducted by simulating two box geometries, namely the first box with a thickness of 4 mm and additional lateral support and the second box with a thickness of 6 mm, it can be said that the thermal load does not significantly affect the maximum total deformation. Of the two designs tested, the first design was the best design based on the maximum total deformation in hydrostatic loading with a water level of 400 mm of 2,170 mm.

5. References

American Society for Testing and Material International (ASTM). (2017). ASTM D790-17: Standard Test Methods for Flexural Properties of Unreinforced and Reinforced Plastics and Electrical Insulating Material. American Society for Testing and Material International (ASTM).

Bayat, S. H., & Nazari, M. B. (2023). Dynamic Crack Analysis in Anisotropic Media Under Wave-like Thermal Loading. European Journal of Mechanics/ A Solids, 99, 1-25. Doi: https://doi.org/10.1016/j.euromechsol.2023.104913

Available online:
http://journal.ipb.ac.id/index.php/jtep
DOI: 10.19028/jtep.012.3.362-375

Badan Standardisasi Nasional. (2020). Konservasi Energi Selubung Bangunan pada Bangunan Gedung, SNI 6389: 2020. Badan Standardisasi Nasional.

Fauzi, I. M., & Hamdhan, I. N. (2019). Analisis Stabilitas Lereng dengan Perkuatan Geotekstil Woven Akibat Pengaruh Termal Menggunakan Metode Elemen Hingga. Rekaracana : Jurnal Teknik Sipil, 2(5), 61-72. Doi: https://doi.org/10.26760/rekaracana.v5i2.61

Hariandja, B. (1997). Mekanika Bahan dan Pengantar Teori Elastisitas. Penerbit Erlangga.

Imanudin, M. S., Bakri, Priatna, S. J., & Kozri, B. (2021). Aplikasi Irigasi Cube Untuk Budidaya Tanaman Tomat Mendukung Smart Irigasi Daerah Perkotaan. Prosiding Seminar Nasional Hari Air Dunia, 6-9. https://conference.unsri.ac.id/index.php/semnashas/article/view/2103

Kadir, F. A. (2005). Analisis Faktor-faktor yang Mempengaruhi Konversi Lahan Sawah ke Penggunaan Non Pertanian di Kabupaten Tangerang [Skripsi]. Institut Pertanian Bogor.

Margolis, J. M. 2006. Engineering Plastics Handbook. McGraw-Hill Education.

Muharomah, R., Setiawan, B. I., Cahrial, E., & Juhaeni, A. H. (2023). Pemberdayaan Kota Tasikmalaya dalam Budidaya Sayuran Menggunakan Fertigator Otomatis Nirdaya (FONi). Jurnal Pengabdian Community, 5(3), 82-87. http://ejournal.ft.unsri.ac.id/index.php/community/article/view/2217

Panggabean, D. S. P., Zakki, A. F., & Arswendo, B. (2015). Perbandingan Penggunaan Material Isotropi dan Orthotropi pada Metode Elemen Hingga untuk Analisa Kekuatan Kapal Fiberglass. Jurnal Teknik Perkapalan, 3(2), 263-272. https://ejournal3.undip.ac.id/index.php/naval/article/view/8601

Pratama, I. H., & Supriyatna, D. (2024). Percobaan Sederhana Tekanan Hidrostatis. Kohesi : Jurnal Multidisiplin Saintek, 3(1), 91-98.

Santoso, E. B., & Widya, R. R. (2014). Gerakan Pertanian Perkotaan dalam Mendukung Kemandirian Masyarakat di Kota Surabaya. Seminar Nasional CITIES 2014, 1-11.

Steawart Jr, M. I. (2014). Surface Production Operations (Third Edition). Gulf Professional Publishing.

Syafriyandi, D., Setiawan, B. I., Arif, C., & Suwardi. (2023). Kinerja Irigasi Bawah Permukaan Otomatis Nirdaya pada Budidaya Kangkung, Caisim, dan Bayam. Jurnal Keteknikan Pertanian, 11(3), 268-278. Doi: https://doi.org/10.19028/jtep.011.3.268-278

Rokhmah, N. A., Ammatillah, C. S., & Sastro, Y. (2014). Vertiminaponik, Mini Akuaponik untuk Lahan Sempit di Perkotaan. Buletin Pertanian Perkotaan, 4(2), 14-22.

Usman, A. S., Rotter, J. M., Lamont, S., Sanad, A. M., & Gillie, M. (2001). Fundamental Principles of Structural Behavior under Thermal Effects. Fire Safety Journal, 36, 721-744. Doi: https://doi.org/10.1016/S0379-7112(01)00037-6

Utami, N., & Cahyo, E. (2022). Sifat Mekanik Komposit Fiberglass Melalui Uji Lentur. Teknika STTKD: Jurnal Teknik, Elektronik, Engine, 8(2), 361-369. https://doi.org/10.56521/teknika.v8i2.798